Pergamon

Journal of Structural Geology, Vol. 17, No. 1, pp. 115 to 129, 1995

0191-8141/95 $9.50 + 0.00

0191-8141(94)E0026-U

Shape preferred orientation of rigid particles in a viscous matrix: re-evaluation to determine kinematic parameters of ductile deformation

TOSHIAKI MASUDA

Institute of Geosciences, Shizuoka University, Shizuoka 422, Japan

KATSUYOSHI MICHIBAYASHI

Department of Geology, James Cook University, Townsville, Qld. 4811, Australia

and

HIROBUMI OHTA*

Institute of Geosciences, Shizuoka University, Shizuoka 422, Japan

(*Received* 19 *December* 1991; *accepted in revised form* 14 *February* 1994)

Abstract—The development of the shape preferred orientation of rigid elliptical bodies during non-coaxial deformation is theoretically simulated in a two-dimensional Newtonian matrix. The angular velocity of a rigid elliptical body ($\dot{\phi}$) can be expressed as

$$\dot{\phi} = \frac{V}{R^2 + 1}\left[R^2 \sin^2\phi \cos\Theta + \cos^2\phi \cos\Theta - (R^2 - 1)\sin^2\phi \sin\Theta\right]$$

where ϕ is the angle between the shear plane and the longest axis of the ellipse, R is the aspect ratio of the ellipse, V is a constant, and Θ is the newly introduced index angle to describe degree of non-coaxiality between simple shear and pure shear defined as $\tan\Theta = \dot{\varepsilon}/\dot{\gamma}$. $\dot{\gamma}$ and $\dot{\varepsilon}$ are simple shear strain rate and pure shear strain rate, respectively. The initial distribution pattern of the elliptical bodies is assumed to be random in an R/ϕ diagram, and a series of the distribution patterns was calculated using the above equation with increasing deformation at varying Θ. When deformation is simple shear (i.e. $\Theta = 0°$), all elliptical bodies rotate with various angular velocities, resulting in a skewed distribution in the R/ϕ diagram. In contrast, for pure shear (i.e. $\Theta = 90°$) all of them asymptotically settle their longest axes on a plane perpendicular to the compression axis, resulting in strongly concentrated and symmetric distribution patterns in the R/ϕ diagram. When deformation is general non-coaxial ($0° < \Theta < 90°$), distribution patterns in the R/ϕ diagram change systematically from the pattern similar to that of $\Theta = 0°$ to that of $\Theta = 90°$ with increasing Θ. These R/ϕ diagrams can be used for estimating the degree of non-coaxiality. We analyzed shape preferred orientation of porphyroclasts in two mylonites, and concluded that deformation within the mylonites contain a certain amount of pure shear component that superimposes on a simple shear component.

INTRODUCTION

Rotation of a rigid ellipsoidal particle embedded in a Newtonian viscous matrix can be quantified by the equations which govern the angular velocity of the particle as a function of the shape parameters of the particle (axial ratio of the ellipsoid) and the mode of the matrix deformation (simple shear, pure shear or a variable non-coaxiality). Jeffery (1922) was the first to establish the general equations and, as an example, gave the expression for simple shear deformation. Gay (1968), based on Jeffery's general equations, presented an alternate expression for pure shear deformation. Ghosh & Sengupta (1973), based on Muskhelishvili's (1953) method for simple problems of elasticity, gave another expression for pure shear deformation. Reed & Tryggvason (1974) calculated the orientations of the longest axis of many ellipsoidal particles subjected to simple and pure shear deformation, and implied that the study of the preferred orientation of rigid particles can supply valuable information to structural geologists. Their analysis, however, appears to be insufficient, partly because they only calculated the orientation of 100 grains with the result that their diagrams of the distribution of the longest axes are not comprehensive. Also, they dealt separately with only simple and pure shear for the matrix deformation. Ghosh & Ramberg (1976) presented a complete analysis for matrix deformation subjected to any combination of simultaneously occurring simple shear and pure shear. Therefore, it is possible to modify Ghosh & Ramberg's analysis to predict the preferred orientation of many rigid ellipsoidal particles for any mode of ductile deformation, which was not performed in Ghosh & Ramberg (1976). Willis (1977) also presented a general kinematic model that can be applied to grains of arbitrary shape, and predicted preferred orientation patterns resulting from rigid rotation. However, his results are probably not easily applicable to naturally deformed rocks, because

*Present address: Kamioka Mining & Smelting Co. Ltd., Kamioka-cho, Yoshiki-gun, Gifu 505-11, Japan.

of difficulties in finding suitable natural data. Passchier (1987) expanded the work of Ghosh & Ramberg (1976) into a three-dimensional analysis of the nature and orientation of asymptotes for rotation of axially symmetric objects in general homogeneous steady flow. He stated that populations of rigid objects in ductilely deformed rocks store a significant amount of information, not only on the sense of vorticity but also on the vorticity number and deviations from plane strain.

In recent years, the study of mylonitic rocks has greatly progressed. One can deduce the shear sense of the deformation on the basis of many criteria such as the shape of mica 'fish', asymmetric pressure shadows, and crystallographic preferred orientation of quartz and other minerals (e.g. Simpson & Schmid 1983, Bouchez *et al.* 1983, Lister & Snoke 1984). In such mylonitic rocks, numerous rigid ellipsoidal grains can be found: feldspar porphyroclasts in quartzose mylonites and pyroxene porphyroclasts in ultramafic mylonites are typical examples (e.g. Nicolas & Poirier 1976, Ramsay & Huber 1987). However, the study of shape preferred orientation of such porphyroclasts in natural rocks has not been particularly fruitful. Oertel (1985) even presented a negative view point for the use of rigid rotation in structural analysis, since the rheological properties of natural materials are presumably not Newtonian. Hanmer (1990) made a similar interpretation that theoretical models for rotation of a rigid ellipsoid may not be directly applicable for natural rocks although they provide insights to study porphyroclast systems.

The purpose of this paper is to re-evaluate rigid rotation as one of the fundamental processes in ductile shear zones, and to emphasize that the shape preferred orientation pattern due to rigid rotation is a useful clue to estimate kinematic parameters of deformation. In this paper, theoretical predictions are made of possible shape preferred orientation patterns for various combinations of simultaneous simple and pure shear, based on the hydrodynamic equations given by Ghosh & Ramberg (1976). The analyses performed are two-dimensional, since the deformation in ductile shear zones can be adequately represented by two dimensions, and these analyses are much simpler than those in three dimensions. Initially, 3600 randomly oriented grains are used in order to obtain clear patterns of the shape preferred orientation. As an application, shape preferred orientation patterns are presented of feldspar and garnet porphyroclasts of two natural mylonitic rocks collected along the Median Tectonic Line of Japan. Attempts are then made to infer kinematic information of the mylonitic deformation by comparing the natural data with the predicted patterns.

THEORY

In the calculation, assumptions are made following Ghosh & Ramberg (1976). The model is two-dimensional, and a rigid elliptical body is considered to be embedded in a two-dimensional Newtonian matrix.

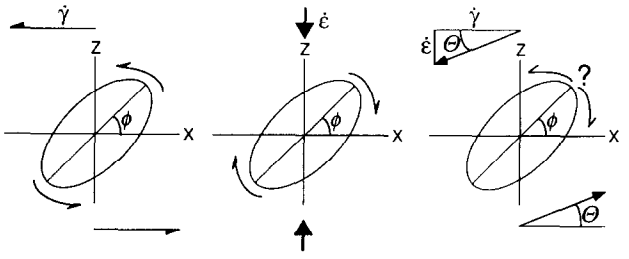

Fig. 1. Schematic drawing of rigid elliptical bodies in a deforming matrix. $\dot{\gamma}$ and $\dot{\varepsilon}$ are the velocities parallel to the x and z axes at ($x = 0$, $z = 1$). (a) Matrix deformation consists of sinistral simple shear. The elliptical body will rotate counterclockwise. (b) Matrix deformation consists of pure shear. The elliptical body will rotate clockwise. (c) Matrix deformation consists of the simultaneous superposition of simple shear and pure shear. The elliptical body will rotate clockwise, keep the same orientation, or rotate counterclockwise depending on ϕ. Θ is defined as the angle between the velocity vector at ($x = 0, z = 1$) and the x axis.

The longest axis of each ellipse will rotate, keeping its origin at ($x = 0$, $z = 0$) in Cartesian co-ordinates. The aspect ratio of the ellipse is termed R. The far-field simple shear component (γ) in the matrix is taken to be sinistral, with the shear plane being parallel to the x axis (Fig. 1a). The far field pure shear component (ε) in the matrix is taken to be compressional in the direction parallel to the z axis and extensional in the direction parallel to the x axis (Fig. 1b).

The velocities in the far-field matrix can be expressed as

$$\left.\begin{aligned} \dot{x} &= \dot{\varepsilon}\, x - \dot{\gamma}\, z \\ \text{and} \qquad \dot{z} &= -\dot{\varepsilon}\, z \end{aligned}\right\} \quad (1)$$

where $\dot{x}$ and $\dot{z}$ are the velocities along the x and z axes, respectively, and $\dot{\gamma}$ and $\dot{\varepsilon}$ are the simple shear strain rate and compressional strain rate, respectively (see Fig. 1). $\dot{\gamma}$ and $\dot{\varepsilon}$ are time-independent constants throughout the deformation.

A kinematical index angle, Θ, is used as a measure of the combination of simple shear and pure shear. Θ is defined as $\tan\Theta = \dot{\varepsilon}/\dot{\gamma}$ ($= s_r$ of Ghosh & Ramberg 1976). Since $\dot{x} = -\dot{\gamma}$ and $\dot{z} = -\dot{\varepsilon}$ at ($x = 0$, $z = 1$), this index angle Θ represents the obliquity of the far-field matrix flow against the x axis at ($x = 0$, $z = 1$) (Figs. 1c and 2a). $\dot{\gamma}$ and $\dot{\varepsilon}$ are expressed by Θ as $\dot{\gamma} = V\cos\Theta$ and $\dot{\varepsilon} = V\sin\Theta$, respectively, where $V = \sqrt{\dot{\gamma}^2 + \dot{\varepsilon}^2}$. V represents the magnitude of the velocity at ($x = 0$, $z = 1$). When the angle $\Theta = 0°$ or $90°$, the flow is either simple shear or pure shear, respectively. The co-ordinate system (Fig. 2a) is different from those by e.g. Passchier (1986), and Wallis (1992) (Fig. 2b). The characteristics of our co-ordinate system is to give the velocity vector at every point by equation (1), and to show the degree of non-coaxiality by the 'anthropocentric' (Hanmer 1990) index angle Θ. Since $\dot{z}/\dot{x} = z/x$ on the apophyses (Fig. 2a), equation (1) results in $z/x = 2\dot{\varepsilon}/\dot{\gamma}$. As $\tan\theta = z/x$ on the apophyses where θ is the angle between flow apophyses, $\tan\theta = 2\tan\Theta$.

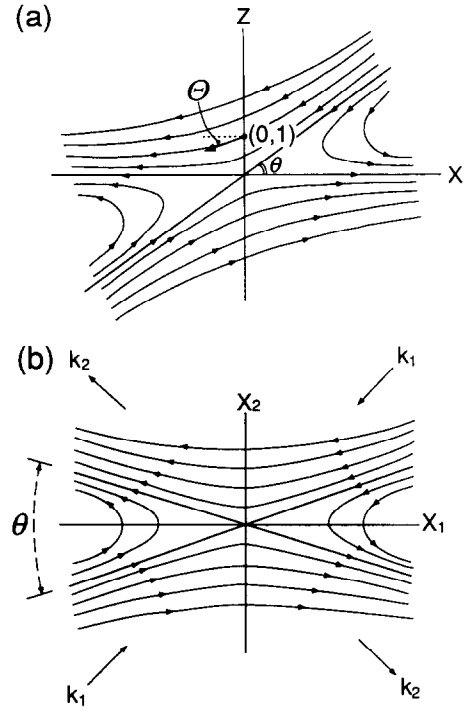

Fig. 2. (a) Co-ordinate system taken in this paper after Ghosh & Ramberg (1976): $\dot{\gamma}$ and $\dot{\varepsilon}$ are the velocity parallel to the x and z axis at ($x = 0$, $z = 1$), respectively. Since $\dot{x} = \dot{\gamma}$ and $\dot{z} = \dot{\varepsilon}$ there, Θ is the angle between the velocity vector and the x axis. (b) Co-ordinate system after Passchier (1986). k_1, k_2 = incremental stretching axes. θ = angle between apophyses.

According to Jeffery (1922), Gay (1968), and Ghosh & Ramberg (1976), the angular velocity of the rigid ellipse due to far-field simple shear $\dot{\phi}_\gamma$ and pure shear $\dot{\phi}_\varepsilon$ can be expressed separately as

$$\dot{\phi}_\gamma = \frac{\dot{\gamma}}{R^2+1}(R^2 \sin^2\phi + \cos^2\phi)$$

and

$$\dot{\phi}_\varepsilon = -\frac{R^2-1}{R^2+1}\dot{\varepsilon}\sin 2\phi$$

where R is the aspect ratio of the ellipse and ϕ is the angle between the longest axis of the ellipse and the x axis (Fig. 1). Thus, the angular velocity for simultaneously occurring simple shear and pure shear, $\dot{\phi}$, is expressed as

$$\begin{aligned}\dot{\phi} &= \dot{\phi}_\gamma + \dot{\phi}_\varepsilon \\ &= \frac{1}{R^2+1}[\dot{\gamma}R^2\sin^2\phi + \dot{\gamma}\cos^2\phi - (R^2-1)\dot{\varepsilon}\sin 2\phi] \\ &= \frac{V}{R^2+1}[R^2\sin^2\phi\cos\Theta + \cos^2\phi\cos\Theta \\ &\quad - (R^2-1)\sin 2\phi\sin\Theta]. \qquad (2)\end{aligned}$$

This equation shows that $\dot{\phi}$ is proportional to V, since the magnitude of $\dot{\phi}$ is controlled by $\dot{\gamma}$ and $\dot{\varepsilon}$. Its detailed interpretations are presented in the next section.

The non-coaxiality of the deformation is expressed as

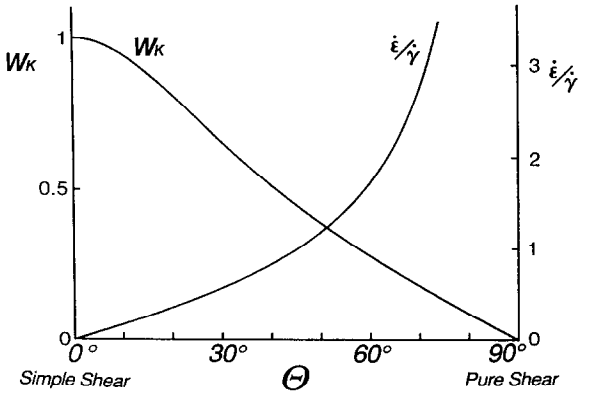

Fig. 3. Measure of non-coaxiality. W_k is the kinematical vorticity number, $\dot{\varepsilon}/\dot{\gamma}$ (= s_r of Ghosh & Ramberg 1975) is the ratio of pure shear strain rate to simple shear rate, and Θ is a kinematical index angle. See the text for the explanation of Θ.

the kinematical vorticity number (W_k; Means *et al.* 1980).

$$W_k = \frac{w}{\sqrt{2(s_1^2 + s_2^2 + s_3^2)}},$$

where w is the vorticity vector and s_1, s_2 and s_3 are the principal strain rates. Ghosh (1987) presented a simple expression for W_k in two dimensions as

$$W_k = \frac{a_{12} - a_{21}}{\sqrt{2}\sqrt{a_{11}^2 + a_{22}^2 + \frac{1}{2}(a_{12}+a_{21})^2}}$$

where a_{11}, a_{12}, a_{21} and a_{22} are constants and in the present case $a_{11} = V\sin\Theta$, $a_{12} = V\cos\Theta$, $a_{21} = 0$ and $a_{22} = -V\sin\Theta$ [compare equation (1) above and equation (2) of Ghosh 1987]. In the strictest sense, the sign of W_k should depend on the sense of shear component [see equation (2) of Ghosh 1987], and sinistral shear requires $W_k < 0$. However, since the sign of W_k is not important here, the constant $a_{12} = V\cos\Theta$ is used instead of $a_{12} = -V\cos\Theta$ in order to obtain $W_k > 0$ for the case of the sinistral shear component. Thus, the kinematical index angle is related to the kinematical vorticity number as

$$W_k = \frac{\cos\Theta}{\sqrt{4 - 3\cos^2\Theta}} = \frac{1}{\sqrt{4\left(\frac{\dot{\varepsilon}}{\dot{\gamma}}\right)^2 + 1}} = \frac{1}{\sqrt{4s_r^2+1}}.$$

The relationship between W_k and Θ is alternatively expressed by following two equations: $W_k = \cos\theta$ (e.g. Passchier 1986) and $\tan\theta = 2\tan\Theta$, where θ is the angle between flow apophyses (see Fig. 2). W_k decreases as Θ increases with a slight deviation from linearity (Fig. 3). In Fig. 3, $\dot{\varepsilon}/\dot{\gamma}$ is also drawn as a function of Θ (i.e. $\dot{\varepsilon}/\dot{\gamma} = \tan\Theta$). The term $\dot{\varepsilon}/\dot{\gamma}$ (= s_r) was used as a measure of non-coaxiality in Ghosh & Ramberg (1976). In this paper however, Θ is preferred to $\dot{\varepsilon}/\dot{\gamma}$ and W_k as a measure of non-coaxiality. Since $\dot{\varepsilon}/\dot{\gamma}$ becomes infinitely large when the mode of deformation approaches pure shear (Fig. 3), it is inconvenient as a measure of the full range of non-coaxiality, from simple shear to pure shear. On the other hand, W_k is a stricter parameter than Θ, but it is more difficult to determine the general nature of the deformation than Θ (cf. Passchier 1987). The pres-

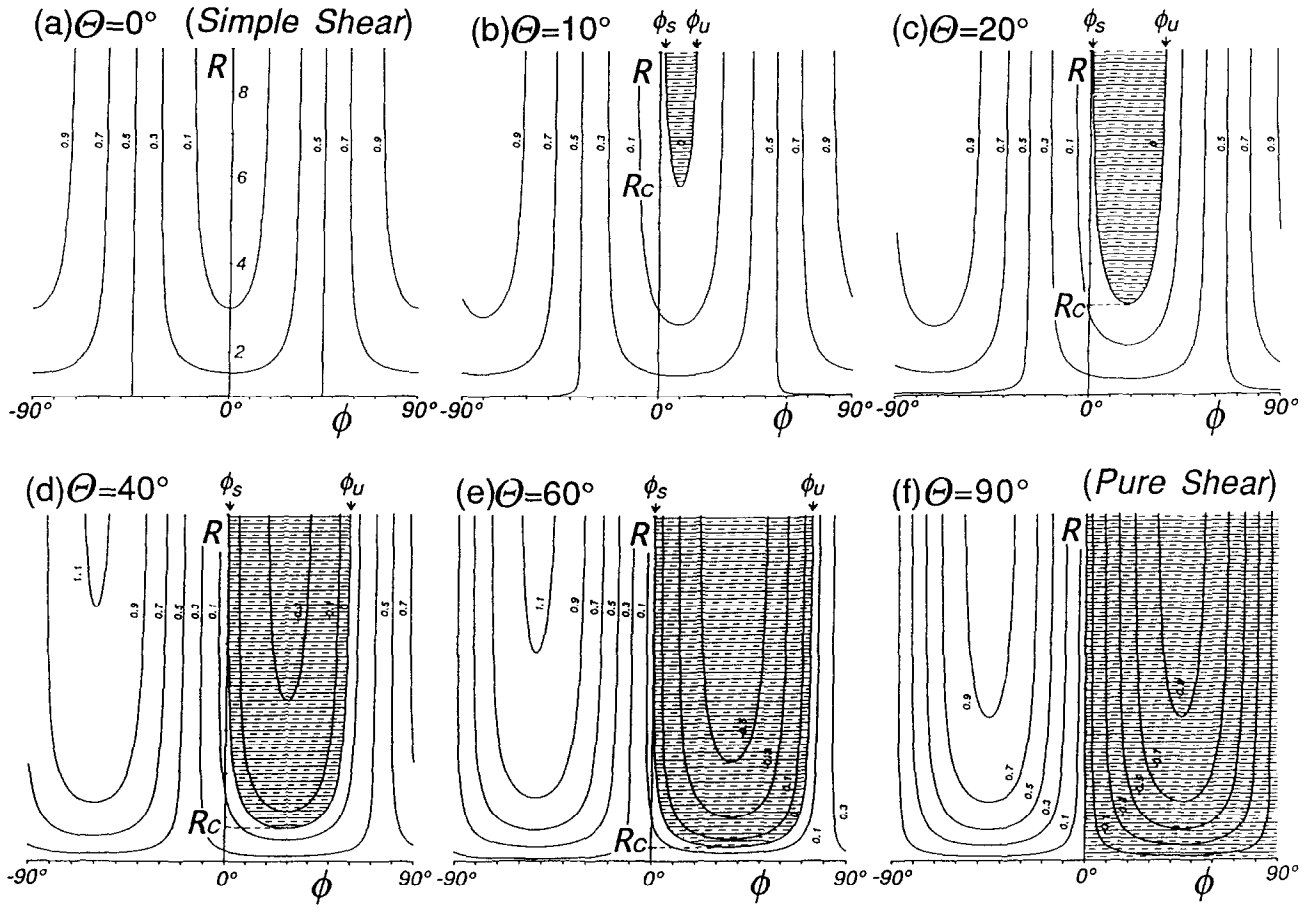

Fig. 4. Contour diagrams of angular velocity in the R/ϕ diagram. Shaded areas indicate negative angular velocity ($\dot{\phi} < 0$), whereas non-shaded areas indicate positive angular velocity ($\dot{\phi} > 0$). R_c shows the critical aspect ratio of each Θ. ϕ_s is the stable critical angles of $\dot{\phi} = 0$, whereas ϕ_u is the unstable critical angles of $\dot{\phi} = 0$. See the text for a detailed description. It is noted that the circular body ($R = 1$) has angular velocity of 0.5, 0.49, 0.47, 0.38, 0.25 and 0 at $\Theta = 0°$, 10°, 20°, 40°, 60° and 90°, respectively.

ent analysis is limited to deformations with non-pulsating histories ($0 \leq W_k \leq 1$: e.g. Means *et al.* 1980; a kinematical dilatancy number $A = 0$, see Passchier 1991). Deformations with pulsating histories ($W_k > 1$: e.g. Means *et al.* 1980) are not dealt with.

It should be noted that the matrix deformation close to the ellipse differs from the far-field matrix deformation. It is implicit that W_k close to the ellipse strongly varies from position to position in the matrix, and that the overall distribution of W_k around the ellipse also varies with time or with the rotation of the ellipse.

ANGULAR VELOCITY

Angular velocity ($\dot{\phi}$) is non-linearly influenced by Θ, ϕ and R, but it is linearly affected by V, as shown by equation (2). In the present calculation of angular velocity, $V = 1$ is assumed. The theoretical analysis is not disturbed by this assumption, since the value of V only controls the time required for the deformation. $\dot{\phi}$ in equation (2) is expressed by a periodic function with respect to ϕ that satisfies $\dot{\phi}(\phi) = \dot{\phi}(\phi + 180°)$. This means that the angular velocity at $\phi = -90°$ is identical to that at $\phi = 90°$.

A detailed description of angular velocity $\dot{\phi}$ as a function of Θ, ϕ and R can be found in Ghosh & Ramberg (1976). In this paper, the contour diagrams of angular velocity with respect to ϕ and R (i.e. R/ϕ diagram) are presented for a series of Θ values (Fig. 4; cf. Passchier 1987).

Simple shear ($\Theta = 0°$)

When the deformation is of simple shear (i.e. $\Theta = 0°$), all the ellipses exhibit positive angular velocity (Fig. 4a), and rotate *always* counterclockwise (e.g. Fig. 1a). The angular velocity for an aspect ratio R maximizes at $\phi = 90°$ and $-90°$, and minimizes at $\phi = 0°$, irrespective of R (Fig. 4a). The contrast between the maximum and minimum angular velocities becomes larger as R increases (Fig. 4a).

Pure shear ($\Theta = 90°$)

For pure shear, the distribution of angular velocity again becomes very simple (Fig. 4f). The ellipses for $\phi > 0°$ have negative angular velocity, whereas those for $\phi < 0°$ have positive angular velocity. The magnitude of the angular velocity is symmetrical with respect to ϕ, and it satisfies $\dot{\phi}(\phi) = -\dot{\phi}(-\phi)$. The absolute value of angular velocity reaches maxima at $\phi = 45°$ and $-45°$ but

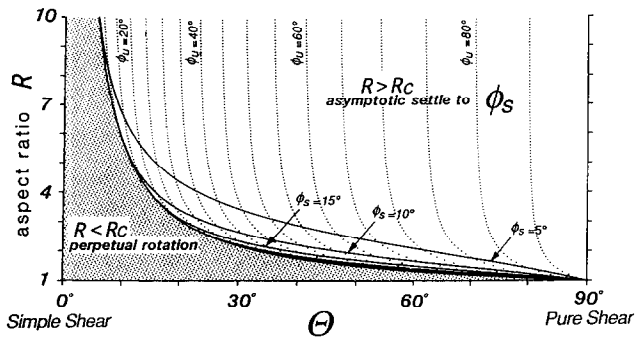

Fig. 5. Critical aspect ratio (R_c) for ϕ_u and ϕ_s. Contours with a 5° interval of ϕ_u and ϕ_s are indicated by dotted and solid lines, respectively. The critical aspect ratio (R_c) is shown as enveloping curve of ϕ_u and ϕ_s in $R - \Theta$ space (i.e. the boundary between the shaded and non-shaded area). Ellipsoidal bodies with $R < R_c$ for each Θ rotate perpetually, whereas those with $R > R_c$ asymptotically settle on the critical angle, ϕ_s.

their directions are opposite one another, whereas the angular velocities at $\phi = 0°$ and 90° are zero ($\dot{\phi} = 0$) so that ellipses will not rotate at these two angles.

General non-coaxial deformation ($0° < \Theta < 90°$)

When the deformation has a simultaneous occurrence of both simple and pure shear, the distribution of angular velocity in the R/ϕ diagram becomes complex (Figs. 4b–e). There is a critical value of the aspect ratio, which is now termed R_c for each Θ (Figs. 4b–e; cf. R_c in Hanmer 1990). The value of R_c with respect to Θ is shown in Fig. 5, which decrease as Θ increases. If an ellipse has smaller aspect ratio than R_c, the angular velocity is positive ($\dot{\phi} > 0$), and therefore the ellipse always rotates counterclockwise (Figs. 4b–e and 6a).

On the contrary, if the ellipse has larger aspect ratios than R_c, the angular velocity will be either positive, zero, or negative depending on the angle (ϕ) and, then, the ellipse will follow one of three different paths: it rotates counterclockwise ($\dot{\phi} > 0$; the non-shaded area in Figs. 4b–e; e.g. Fig. 6b), remains stable ($\dot{\phi} = 0$; the boundary between the non-shaded and shaded areas in Figs. 4b–e; e.g. Figs. 6d & e), and rotates clockwise ($\dot{\phi} < 0$; the shaded area in Figs. 4b–e; e.g. Fig. 6c), respectively (cf. Passchier 1987, Hanmer 1990, Hanmer & Passchier 1991).

As shown in Figs. 4(b)–(e), these three paths are bounded by the contour line of $\dot{\phi} = 0$. This contour line results from two different critical values of ϕ that theoretically satisfy $\dot{\phi} = 0$ in relation to equation (2) for each R. In this paper, they are called as ϕ_u and ϕ_s ($\phi_u > \phi_s$; e.g. Fig. 6). The value of ϕ_u and ϕ_s are between 0° and 90° and their difference becomes larger as R increases (Figs. 4b–e and 5). When the angle of an ellipse lies between ϕ_u and ϕ_s, the angular velocity is negative so that the ellipse rotates clockwise towards ϕ_s (e.g. Fig. 6c). When the angle is smaller than ϕ_s or larger than ϕ_u, the angular velocity is positive so that the ellipse rotates counterclockwise towards ϕ_s (Fig. 6b). Consequently, most ellipses, that satisfy $R > R_c$, will rotate asymptotically towards ϕ_s during non-coaxial deformation.

The only exception is the ellipses which are oriented exactly parallel to ϕ_u before deformation (e.g. Fig. 6e). As these ellipses have $\dot{\phi} = 0$, they do not change their orientation during deformation. However, if the orientation of an ellipse is only very slightly oblique to ϕ_u, the ellipse will rotate towards ϕ_s. This is because ϕ_s is the stable critical angle, whereas ϕ_u is the unstable critical angle. ϕ_s is the orientation of the rest position of Hanmer (1990) and Hanmer & Passchier (1991), and stable sink position of Passchier (1987).

In the special case when $R = R_c$, there is only one value of ϕ that satisfies the relation $\dot{\phi} = 0$ in equation (2). In this case ϕ_u is considered to be identical to ϕ_s, and there is no angle for ellipse to have negative angular vorticity (Figs. 4b–e and 5).

CALCULATION OF THE CHANGE OF ϕ WITH DEFORMATION

Taking an ellipse oriented with ϕ_0, the new orientation (ϕ_1) of the ellipse after a very short time (dt) can be expressed as

$$\phi_1 = \phi_0 + \dot{\phi}_0 dt$$

where $\dot{\phi}_0$ is angular velocity at $\phi = \phi_0$. In the same manner, the orientation of the ellipse after the next dt is known as

$$\phi_2 = \phi_1 + \dot{\phi}_1 dt$$

where ϕ_2 is the new orientation and $\dot{\phi}_1$ is angular velocity at $\phi = \phi_1$. As $dt \rightarrow 0$, the manner in which ϕ changes can be smoothly traced by repeating this calculation. The above calculation has been repeated, setting $dt = 0.01$.

Simple shear strain γ and pure shear strain ε are defined as

$$\gamma = \int \dot{\gamma} dt$$

and

$$\varepsilon = \int \dot{\varepsilon} dt,$$

respectively. Therefore, the magnitude of strain for general deformation can be analogously defined as

$$D' = \int \sqrt{\dot{\gamma}^2 + \dot{\varepsilon}^2}\, dt.$$

D' is directly given by a number of repetitions of the above calculation, and is exactly equivalent to γ or ε when the deformation is of simple shear or pure shear, respectively. In our case $D' = 1$ is reached by 100 repetitions of the calculation, as we set $V = \sqrt{\dot{\gamma}^2 + \dot{\varepsilon}^2} = 1$ and $dt = 0.01$. Strain magnitude, $\overline{\varepsilon_s}$ (Nadai 1963), is given by

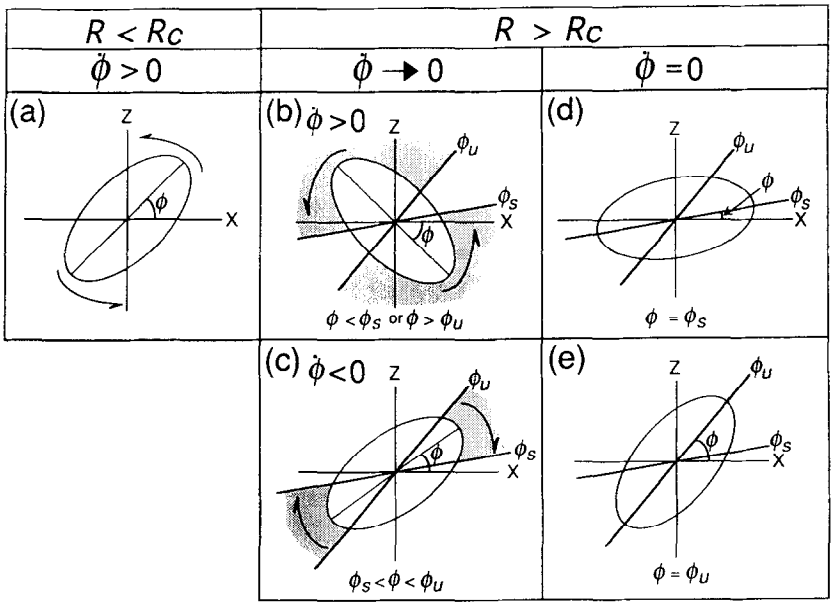

Fig. 6. Schematic drawing of rigid elliptical bodies in a non-coaxial deforming matrix ($0° < \Theta < 90°$). The simple shear component is sinistral. (a) If the elliptical body has an aspect ratio smaller than the critical one (i.e. $R < R_c$), angular velocity is always positive ($\dot{\phi} > 0$) so that it will always rotate counterclockwise. (b) & (c) The elliptical body has an aspect ratio greater then the critical one (i.e. $R > R_c$). Its rotation depends on the angle of its longest axis (ϕ) with respect to the critical angles of ϕ_s and ϕ_u. (b) If the angle is smaller than ϕ_s or greater than ϕ_u, angular velocity is positive (shaded areas) so that the elliptical body will rotate counterclockwise towards ϕ_s. (c) If the angle of its longest axis is between ϕ_s and ϕ_u, angular velocity is negative (shaded area) so that the elliptical body will rotate clockwise towards ϕ_s (i.e. back rotation). (d) & (e) Special cases happen when the elliptical body has an aspect ratio greater than or equal to the critical angle (i.e. $R > R_c$). (d) If the angle of its longest axis is equal to ϕ_s, the ellipse will not rotate at all. (e) If the angle is exactly equal to ϕ_u, it will not rotate, either. However, even if the angle is only slightly oblique to ϕ_u it will rotate towards ϕ_s.

$$\bar{\varepsilon}_s = \frac{1}{\sqrt{3}}[(\varepsilon_1 - \varepsilon_2)^2 + (\varepsilon_2 - \varepsilon_3)^2 + (\varepsilon_3 - \varepsilon_1)^2]^{1/2}$$

where ε_1, ε_2 and ε_3 are natural or logarithmic principal strains. In our case, $\varepsilon_2 = 0$ and $\varepsilon_1 = -\varepsilon_3$. Therefore

$$\bar{\varepsilon}_s = \sqrt{2}\,\varepsilon_1 = \sqrt{2}\ln R_1 \qquad (3)$$

where R_1 is the semi-major axis of the strain ellipse far from the rigid ellipse, which was given by Ghosh (1987):

$$R_1 = \frac{1}{2}\left[\left\{4 + \left(4 + \frac{1}{s_r^2}\right)\sinh^2(\gamma s_r)\right\}^{1/2} + \left\{\left(4 + \frac{1}{s_r^2}\right)\sinh^2(\gamma s_r)\right\}^{1/2}\right].$$

As $\gamma = D' \cos\Theta$ and $s_r = \sin\Theta/\cos\Theta$,

$$R_1 = \frac{1}{2}\left[\left\{4 + \left(4 + \frac{1}{s_r^2}\right)\sinh^2(D' \sin\Theta)\right\}^{1/2} + \left\{\left(4 + \frac{1}{s_r^2}\right)\sinh^2(D' \sin\Theta)\right\}^{1/2}\right] \qquad (4)$$

equations (3) and (4) give the relationship between $\bar{\varepsilon}_s$ and D'.

COMPUTER MODELLING OF PREFERRED ORIENTATION OF ELLIPSES

It is assumed that the angular velocities of ellipses, which are dealt with in the calculation, are individually controlled by equation (2), with no interaction among them. The longest axes of the ellipses before deformation are set to be homogeneously spaced from $\phi = -90°$ to 90° with a 0.2 interval and R from 1 to 9 with a 0.2 interval. Thus, the total numbers of the ellipses in the R/ϕ diagram are 3600 grains (see Fig. 7a).

As deformation occurs the ellipses rotate and their orientations change, resulting in an inhomogeneous distribution of ϕ for the ellipses. The plotted points for an ellipse in the R/ϕ diagrams (Figs. 7–13) move horizontally, because ϕ changes while R does not change during deformation. Seven cases of Θ were analyzed (i.e. $\Theta = 0°$, 10°, 20°, 40°, 60°, 80°, and 90°) as shown in Figs. 7–13. The degree of concentration in the orientation (ϕ) is expressed by the density of points in the diagrams.

Simple shear ($\Theta = 0°$)

In the case of simple shear ($\Theta = 0°$; Fig. 7) where all the ellipses rotate counterclockwise during deformation (e.g. Fig. 1a), the concentration pattern varies gradually and becomes complex as time or strain increases. At low strains ($\gamma \leq 3$), an obvious concentration of ϕ is located around −10° to −20°; the concentration is more prominent for larger R (e.g. $\gamma = 3$ in Fig. 7).

As the strain increases in the range $3 < \gamma < 6$, a belt of concentrated points in the R/ϕ diagram becomes clear (e.g. $\gamma = 4$ in Fig. 7). The center of the concentrated area is around $\phi = -10°$ for larger R ($R > 4$), whereas it is found in the positive range of ϕ for smaller values of R

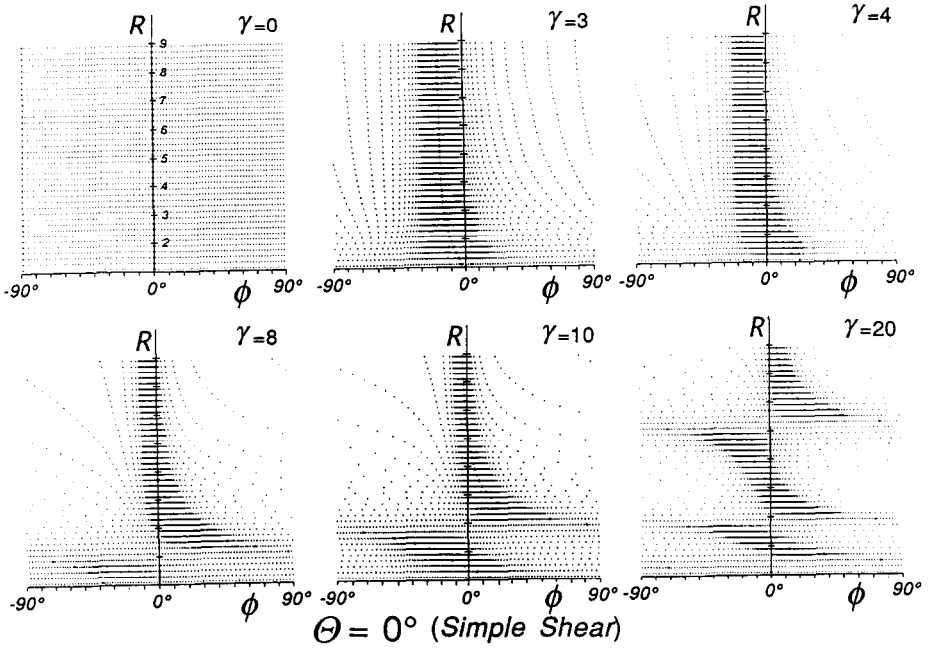

Fig. 7. Distribution patterns of the longest axes of ellipses in the R/ϕ diagram for simple shear ($\Theta = 0°$) with respect to γ. Horizontal and vertical axes indicate orientation (ϕ) and aspect ratio (R), respectively. Large dots as markers show ellipses whose initial orientations were −89°.

($2 < R < 3$). The degree of concentration is denser at large values of R. However, it is very sparse at $R < 1.5$ where the center of the concentrated points cannot be easily detected.

For a strain value of $\gamma = 8$ the concentration at $R < 2$ becomes obscure (Fig. 7). When $\gamma = 10$, the belt of concentration in the R/ϕ diagram is split into two parts at $R = 3$ (Fig. 7). The belt above $R = 3$ lies in the top-center to bottom-right region. The belt below $R = 3$ is formed in the area from the top-left to bottom-center. The position of concentrated points of ϕ shifts to the right as γ increases. When $\phi = 90°$ is reached, it also appears at $\phi = -90°$ for further increases in γ. At $\gamma = 20$, the belt of concentrated points is clearly split into three parts with respect to R (Fig. 7). This means three different preferred orientations for different shaped elliptical bodies.

Pure shear ($\Theta = 90°$)

In the case of pure shear, all the orientations of the ellipses tend to gather at $\phi = 0°$ (Fig. 8). Since the angular velocity is greater at larger values of R (Fig. 4f), the degree of concentration is higher at larger values of R. The distribution pattern in the R/ϕ diagram is symmetrical at $\phi = 0°$ for all values of ε (Fig. 8). By $\varepsilon = 4$, most of ellipses having $R > 2$ are already concentrated on the shear plane (Fig. 8).

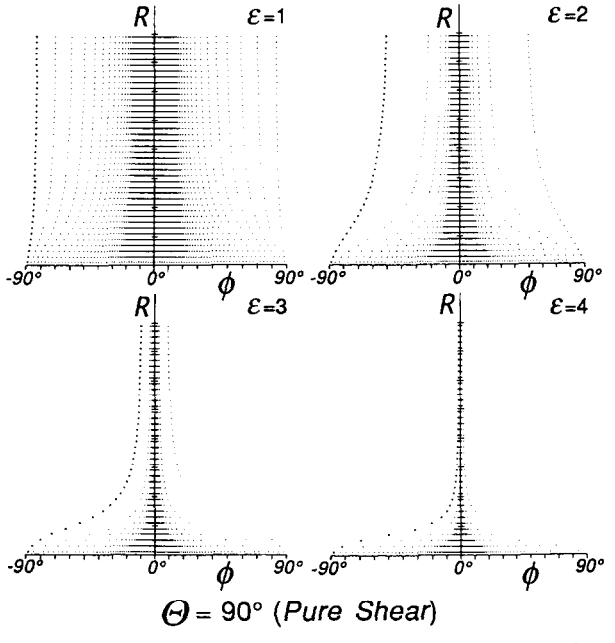

Fig. 8. Distribution patterns in the R/ϕ diagram for pure shear ($\Theta = 90°$). They are symmetric with respect to $\phi = 0°$. Note that ellipses of $R > 2$ settle asymptotically on $\phi = 0°$ by $\varepsilon = 4$.

General non-coaxial deformation ($0° < \Theta < 90°$)

For the cases when $0° < \Theta < 90°$ where both the simple shear and pure shear occur simultaneously, the distribution patterns in the R/ϕ diagram vary depending on Θ (Figs. 9–13). When $\Theta = 10°$, the pattern of distribution is similar to that of simple shear, particularly with respect to ellipses having smaller aspect ratios where the belt of concentration is split into two parts with increasing strain as those for simple shear (cf. Fig. 9 with Fig. 7). This pattern does not occur when Θ is larger than or equal to 20°. When $\Theta = 20°$, the distribution of ellipses having $R > 2$ concentrates as the strain increases, while those having $R < 2$ lose their concentration by $D' = 8$ (Fig. 10).

As the value of Θ increases, the distribution patterns become more similar to those for pure shear. When Θ is

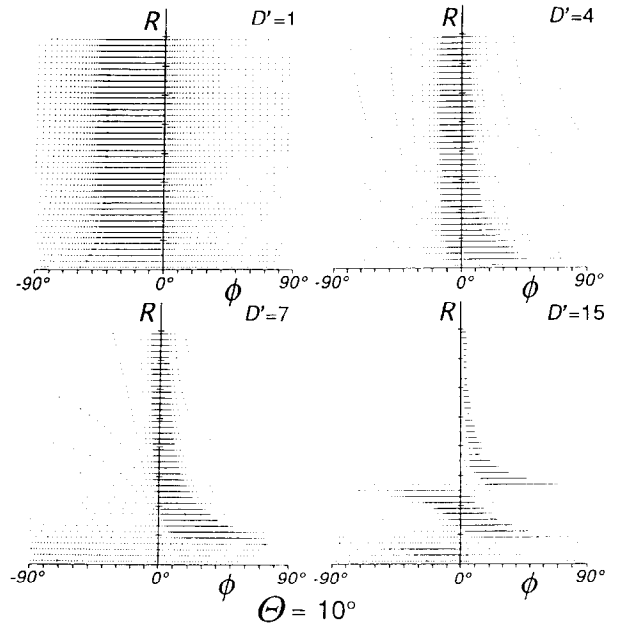

Fig. 9. Distribution patterns in the R/ϕ diagram for $\Theta = 10°$. The patterns of the ellipses of $R \leq 4$ are similar to those for simple shear in Fig. 7. The patterns of the ellipses of $R \leq 2$ become obscure at $D' = 7$. In contrast the ellipses of $R > 4$ asymptotically settle on a belt of concentration at $D' = 15$. $\overline{\varepsilon_s} = 0.7, 2.2, 3.2$ and 5.2 for $D' = 1, 4, 7$ and 15, respectively.

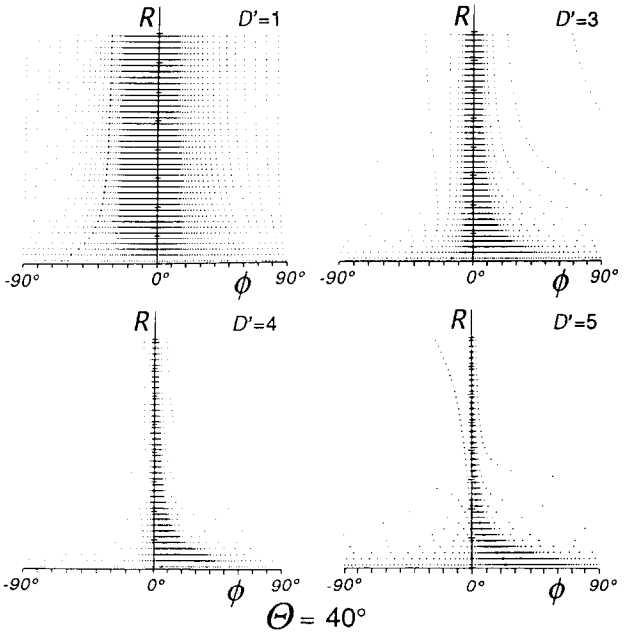

Fig. 11. Distribution patterns in the R/ϕ diagram for $\Theta = 40°$. The patterns result asymptotically in a belt of concentration by $D' = 4$. $\overline{\varepsilon_s} = 1.0, 2.9, 3.8$, and 4.8 for $D' = 1, 3, 4$ and 5, respectively.

larger than or equal to 40°, ellipses that have R greater than R_c, are clearly apt to approach the critical angle, ϕ_s, so that their distribution patterns results in a belt of concentration (Figs. 11–13). This concentration can take place only by $D' = 4$ (Figs. 11–13; cf. Fig. 8), suggesting that their distribution patterns are almost stable with increasing strain (cf. Passchier 1987). In contrast, ellipses having R smaller then R_c always rotate (Figs. 4, 5 and 6a), although their distribution patterns are rather asymmetric with respect to $\phi = 0$ when Θ is smaller than 80° (e.g. Figs. 9–12; cf. Hanmer 1990). When $\Theta = 80°$, their distribution patterns are very similar to those for pure shear (cf. Fig. 13 with Fig. 8).

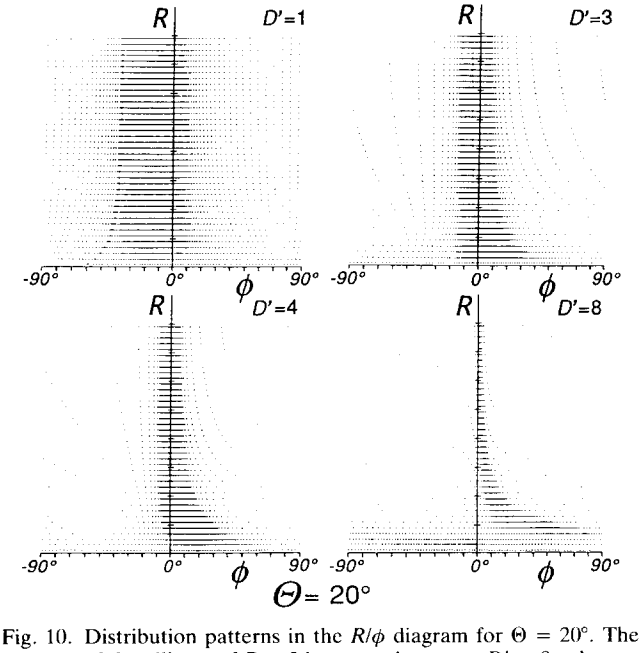

Fig. 10. Distribution patterns in the R/ϕ diagram for $\Theta = 20°$. The patterns of the ellipses of $R \leq 2$ become obscure at $D' = 8$, whereas those of $R > 2$ asymptotically settle on a belt of concentration. $\overline{\varepsilon_s} = 0.8, 2.1, 2.6$ and 4.6 for $D' = 1, 3, 4$ and 8, respectively.

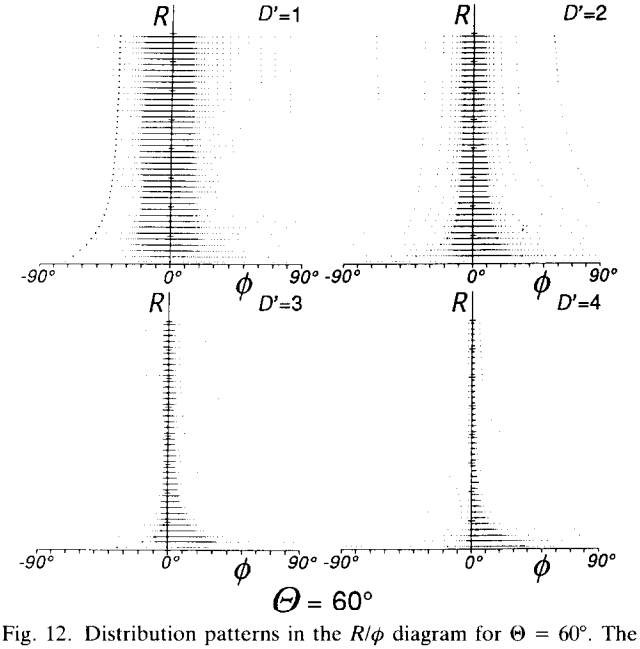

Fig. 12. Distribution patterns in the R/ϕ diagram for $\Theta = 60°$. The patterns result asymptotically in a belt of concentration by $D' = 4$. Its degree of the concentration is higher than those for $\Theta = 40°$ in Fig. 11. $\overline{\varepsilon_s} = 1.3, 2.5, 3.7$ and 5.0 for $D' = 1, 2, 3$ and 4, respectively.

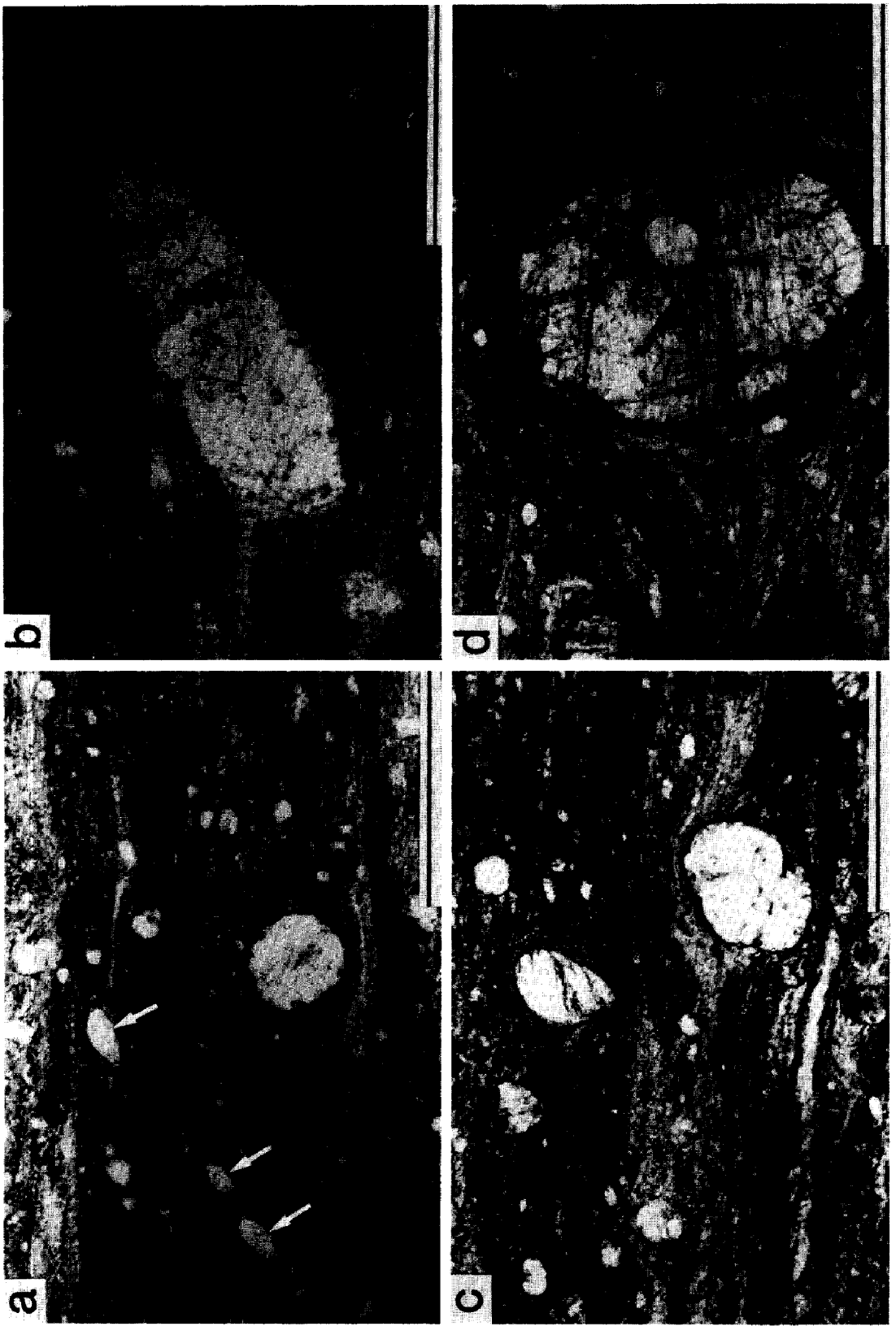

Fig. 14. Photomicrograph (open nicol) of the Ohnishiyama mylonite. Scale bar = 1 mm. Shear sense is sinistral in the photomicrographs. All the porphyroclasts are feldspar grains, whose shapes in the cross-section are approximately represented by ellipses. Light colored layers are rich in quartz and feldspar grains, whereas the darker layers are rich in mica grains. (a) Note that most porphyroclasts have no clear tails. Elliptical porphyroclasts (indicated by arrows) are arranged with the opposite orientation to those of ideal mica fish, if present. (b) This porphyroclast system appears to have tails and is assigned to the σ-type. (c) Most porphyroclasts have no clear tails. Asymmetric pressure shadows which indicate a sinistral shear sense can be seen around the large porphyroclasts. (d) Note that minor folds can be seen at both sides of the porphyroclast. The porphyroclast appears to have been rotated.

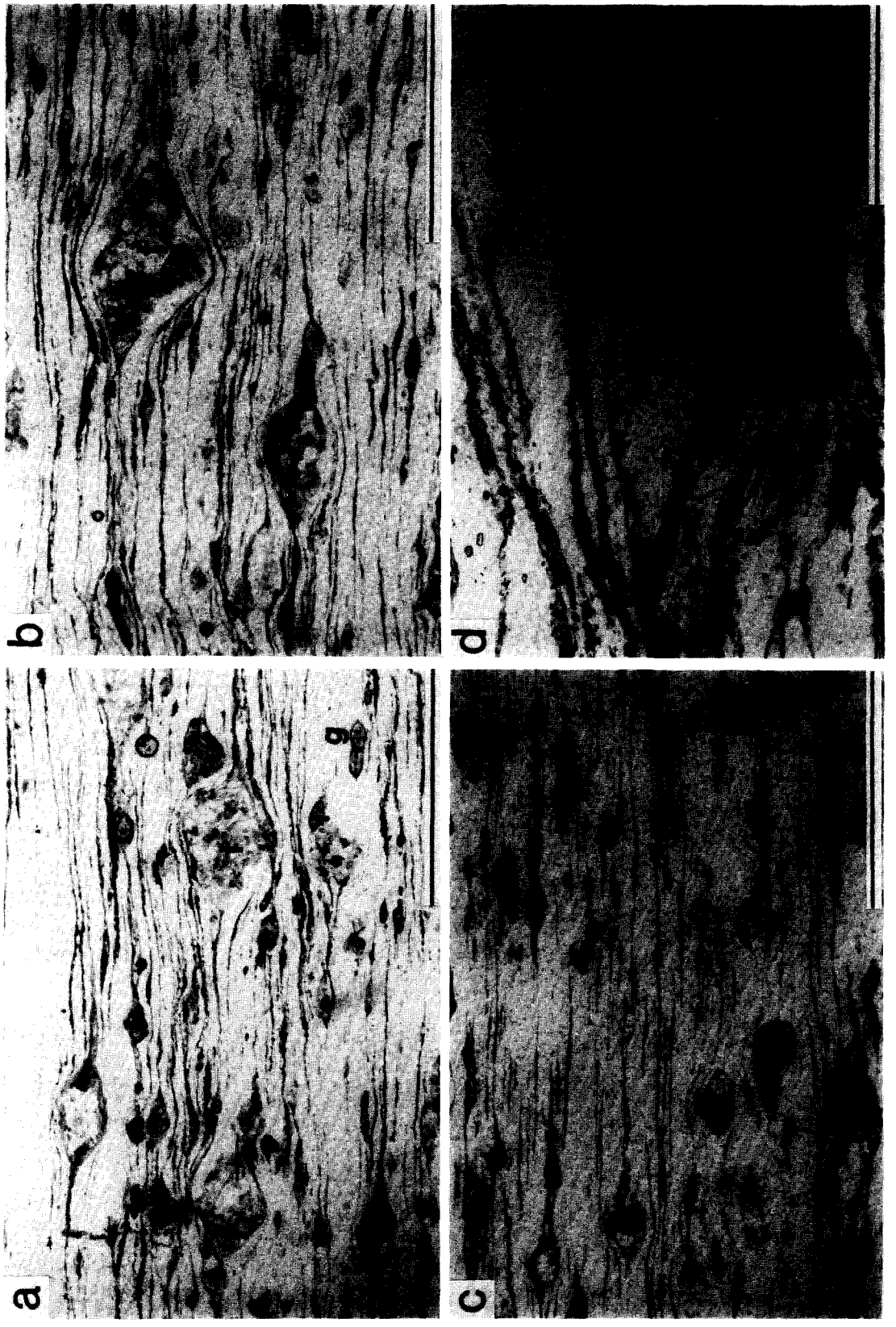

Fig. 15. Photomicrograph (open nicol) of the Yanazawa mylonite. Scale bar = 1 mm for (a)–(c), and 0.2 mm for (d). Typical grains of feldspar and garnet are labeled as f and g, respectively. Thin mica films (in black) define the foliation. The matrix (in white) consists of quartz. The shear sense is sinistral. (a)–(c) Asymmetric pressure shadows indicated by deflection of mica layers can be seen around the larger feldspar porphyroclasts. Garnet grains with large aspect ratios tend to arrange their longest axes parallel to the foliation. No tails can be seen around feldspar nor garnet porphyroclasts. (d) Mica (muscovite) fish indicating a sinistral shear sense.

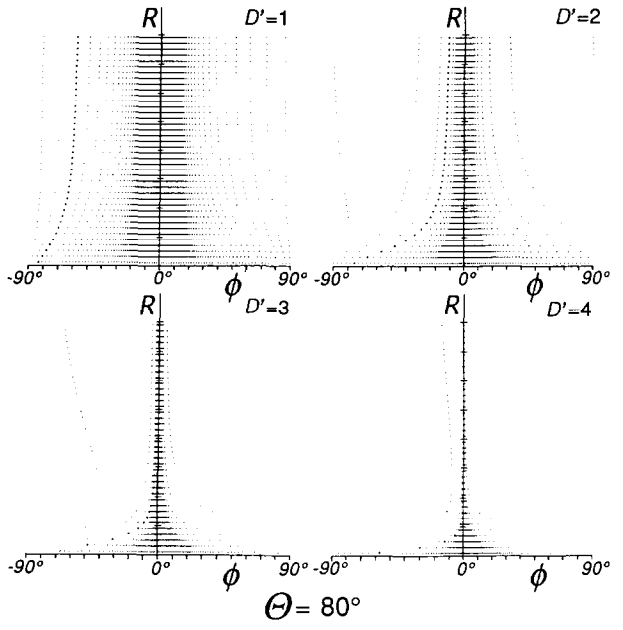

Fig. 13. Distribution patterns in the R/ϕ diagram for $\Theta = 80°$. They are quite similar to those for pure shear ($\Theta = 90°$) shown in Fig. 8. $\overline{\varepsilon_s} = 1.4$, 2.8, 4.2 and 5.6 for $D' = 1$, 2, 3 and 4, respectively.

APPLICATION OF THEORETICAL MODELLING TO MYLONITES

The theoretical distribution of shape preferred orientation of the rigid elliptical bodies presented above can be used to estimate both non-coaxial index angle, Θ, and strain, D' (or $\overline{\varepsilon_s}$), for mylonites in nature. In this section, the orientation and aspect ratio of elliptical porphyroclasts (feldspar and garnet) in two mylonites are analyzed as an example.

Geological setting

Two mylonite samples were collected from Ohnishiyama and Yanazawa within the Kashio Shear Zone along the Median Tectonic Line in central Honshu, Japan. The Ohnishiyama mylonite was derived from early Cretaceous Hiji tonalite (e.g. Hayama & Yamada 1980), whereas the Yanazawa mylonite was derived from a Ryoke metachert (Michibayashi & Masuda 1993). The metacherts in the Ryoke metamorphic belt were originally deposited as bedded-cherts as members of the Jurassic accretionary complex (e.g. Mizutani 1987), and were subsequently transformed into metacherts during the early Cretaceous Ryoke metamorphic event (e.g. Miyashiro 1973).

The mylonitic deformation took place during the late Cretaceous to early Tertiary age (e.g. Hayama & Yamada 1980, Shibata & Takagi 1987, Dallmeyer & Takasu 1992). Mylonitic foliation generally strikes NNE–SSW and dips, mostly at high angles, to the west. Mylonitic lineation on the foliation surface trends NNE–SSW and plunges gently towards north. The Median Tectonic Line strikes approximately NNE–SSW and dips vertically, and the trajectories of the mylonitic foliation are transected by the Median Tectonic Line with a slight obliquity (e.g. Takagi 1986). The shear sense of the mylonites was deduced as sinistral or top-to-the-south (e.g. Takagi 1986, Hayashi & Takagi 1987, Michibayashi & Masuda 1993, Yamamoto 1994), based on microstructural criteria (e.g. Berthe *et al.* 1979, Simpson & Schmid 1983, Lister & Snoke 1984).

Microstructure of the mylonites

Thin sections were made in a plane parallel to the lineation and perpendicular to the foliation. A brief description of the microstructures follows.

The Ohnishiyama mylonite. In Fig. 14, the mylonite appears porphyroclastic. The porphyroclasts, consisting predominantly of plagioclase with rare K-feldspar, appear to be approximately elliptical in section, with grain size between several hundreds of microns to two millimeters. The matrix consists of a fine-grained mixture of quartz, plagioclase, K-feldspar and micas. The matrix foliation is defined by the banding of quartz and feldspar rich, and mica rich layers (Fig. 14).

Most porphyroclast systems do not have conspicuous tails of feldspar that could result from recrystallization of the host grain. Instead, they are commonly surrounded by the other minerals such as fine grained quartz and micas (Fig. 14; cf. Takagi & Ito 1988). Their geometries are similar to θ-type described by Hooper & Hatcher (1988). They can be divided into two subtypes; one involves the embayment of foliation, whereas the other does not exhibit a remarkable embayment of foliation (Fig. 14). The former subtype appears to have been developed around porphyroclasts with circular and weakly elliptical cross-sections (e.g. Fig. 14d), whereas the latter subtype usually developed around porphyroclasts having larger aspect ratios (e.g. Fig. 14b). Locally, porphyroclasts occur with some tails. Their geometries are commonly similar to σ-type of Passchier & Simpson (1986), but no clear δ-type have been observed.

The Yanazawa mylonite. The Yanazawa mylonite is composed of quartz, plagioclase, K-feldspar, muscovite, biotite, garnet, apatite and tourmaline. The foliation can be defined by the parallel arrangement of the mica flakes. Plagioclase and garnet grains occur as porphyroclasts, and are surrounded by a fine grained matrix of quartz and micas (Fig. 15). Plagioclase grains are larger than the matrix quartz grains, and are well represented by ellipses (Fig. 15), the longest axis of which is a few hundreds of microns. Garnet grains, that are relatively larger than the feldspar, show local elliptical shapes with longest axis oriented parallel to the foliation. Their porphyroclast systems occur with and without tails. Tails occupy at most a few percent of the area (volume) of their host porphyroclasts (Fig. 15). This indicates that recrystallization of the host porphyroclast resulted moderately in the fine-grained tails. Their geometries are similar to the σ-type, but few δ-type geometries are apparent (Fig. 15). In contrast, the porphyroclast systems without tails usually have slightly asymmetric

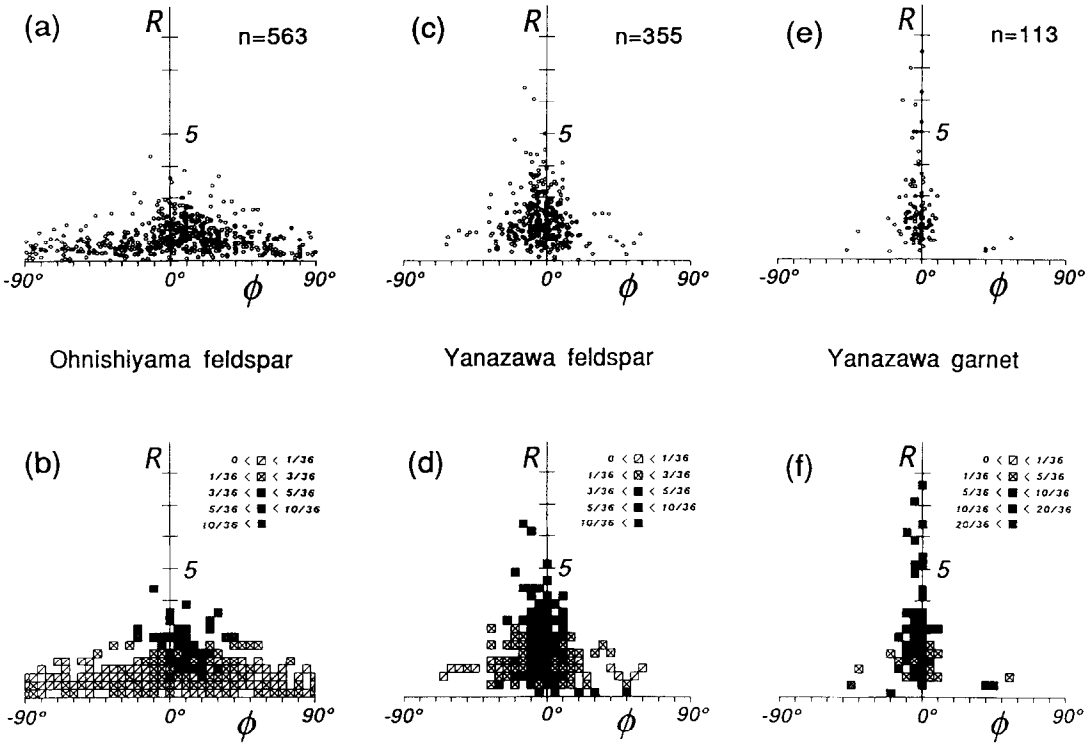

Fig. 16. Distribution patterns (a), (c) & (e) and number distribution patterns (b), (d) & (f) of the longest axes of porphyroclasts measured in the mylonites. (a) & (b) feldspar porphyroclasts within the Ohnishiyama mylonite, (c) & (d) feldspar porphyroclasts within the Yanazawa mylonite, and (e) & (f) garnet porphyroclasts within the Yanazawa mylonite. See text for an explanation.

pressure shadows which consist predominantly of micas and quartz (Fig. 15c), and their geometries are similar to the θ-type.

Measurement of porphyroclasts

The longest axis of each porphyroclast can be easily recognized, which allows measurement of the aspect ratio defined as the longest/shortest axes of the ellipse in the photomicrographs. The orientation of the longest axis with respect to the foliation is also measured, with the error of less than ±5°. The error is mainly due to the slight undulation of the foliation.

Figure 16 shows the results of the measurements with the numbers of each orientation. Each density distribution is shown in Figs. 16(b), (d) & (f). The density is determined as the ratio of the number of grains in a particular orientation (ϕ) to the total number of grains, for the same range of R. These R/ϕ diagrams and their density distribution diagrams (Fig. 16) are compared with the theoretically predicted distribution patterns such as those in Figs. 7–13.

Aspect ratios of feldspar porphyroclasts within the Ohnishiyama mylonite are dominantly in the range of 1 to 3 (Fig. 16a). For $1 < R < 2$, the orientation of the longest axis (ϕ) is distributed homogeneously from −90° to 90°. For $R > 2$ the distribution of ϕ skews on the positive side and angle of their concentrations gradually changes from higher angle to zero as R increases (Fig. 16b). Taking these features into account, Θ should be determined to be less than or equal to 20°, since these values of Θ can only produce such a homogeneous distribution (Figs. 7, 9 and 10). We found by eye that the distribution of $D' = 4$ ($\overline{\varepsilon_s} = 2.62$, $R_1 = 6.40$) where $\Theta = 20°$ is the most similar pattern and that of $D' = 4$ ($\overline{\varepsilon_s} = 2.20$, $R_1 = 4.73$) where $\Theta = 10°$ is the next. Any distribution patterns for simple shear ($\Theta = 0°$) does not resemble the Ohnishiyama pattern.

Feldspar porphyroclasts within the Yanazawa mylonite (Figs. 16c & d) are distributed in a relatively narrower range of the angle (ϕ). For $R < 2$ the range of ϕ of the feldspar porphyroclasts is found to be between −70° to 70°, whereas for $R > 2$ the range becomes much narrower. The aspect ratio of feldspar is mostly around 2.0. We found by eye that it is very difficult to fit this distribution pattern to those where Θ is smaller than or equal to 20°. The theoretical distribution for $D' = 5$ ($\overline{\varepsilon_s} = 4.75$, $R_1 = 28.9$) and $\Theta = 40°$ is most similar to the Yanazawa mylonite pattern.

The ϕ and R of garnet porphyroclasts within the Yanazawa mylonite are plotted in Fig. 16(e), which shows that the aspect ratios (R) of garnet are larger than those of feldspar, whereas the range of the angle (ϕ) is much narrower than that of feldspar. Most garnet porphyroclasts are oriented in the range between −20° and 20° (Figs. 16e & f).

Passchier (1987) proposed a method for estimating degree of non-coaxiality by measuring orientation of stable sink position (i.e. ϕ_s). The method was not applied to our mylonites, because we cannot recognize which porphyroclast is in the stable sink position.

VALIDITY OF THEORETICAL ASSUMPTIONS TO THE MYLONITES

The results that $D' = 4$ and $\Theta = 20°$ for the Ohnishiyama mylonite and $D' = 5$ and $\Theta = 40°$ for the Yanazawa mylonite were obtained with the following assumptions: (1) the matrix of the mylonites is represented by a Newtonian viscous material; (2) the initial orientations of the rigid minerals (feldspar and garnet) were random; (3) no change in the shape of the porphyroclasts occurred during the deformation; and (4) no interaction occurred between porphyroclasts. As these assumptions are very critical, the obtained results may require some revision.

Oertel (1985) pointed out that the rheological properties of rocks are hardly Newtonian and that different rheological properties of the matrix produce different results (see also Hanmer & Passchier 1991). Considering a non-Newtonian viscous matrix, discussion is focused on what kind of revision should be required to modify the calculation for a Newtonian matrix.

Equations which yield the angular velocity for a non-Newtonian matrix can be expressed by the equations for a Newtonian matrix with the additional term which characterizes the oddness of the non-Newtonian behavior (Leal 1975). Theoretical studies have shown that for simple shear an ellipsoidal particle will perpetually rotate in the non-Newtonian matrix, whereas for pure shear its long axis will asymptotically approach the perpendicular to the direction of compression (e.g. Leal 1975), as can be seen for the Newtonian matrix in this paper. Thus, for the simultaneous superposition of simple and pure shear, critical angles of orientation should also exist, depending on the aspect ratio of the ellipse and non-coaxiality of deformation, which give zero angular velocity such as ϕ_u and ϕ_s for the Newtonian matrix. This means that the general scheme obtained for a Newtonian matrix is applicable to a non-Newtonian matrix, and that Figs. 7–13 are qualitatively acceptable as a first approximation. Ferguson (1979) stated the positive view that Jeffery's (1922) Newtonian model is likely to be good approximation for non-Newtonian matrix except for very large strain. Therefore, the values of ϕ_u and ϕ_s for a Newtonian matrix are likely to be good approximation for a non-Newtonian matrix.

Assumption (2), that the initial orientation was random, may be generally acceptable for minerals in massive igneous rocks but unacceptable for minerals in well foliated and lineated metamorphic rocks. Since the Ohnishiyama mylonite is considered to be derived from granodiorite or tonalite (Hayama & Yamada 1980), assumption (2) is probably satisfied. However, it is rather doubtful whether the feldspar and garnet grains within the Yanazawa mylonite satisfy assumption (2) by being random. To check the initial preferred orientations of the feldspar and garnet grains, an examination was made of several Ryoke metacherts from the Hongusan area (see Masuda *et al.* 1991), which were collected far from the Median Tectonic Line and are not mylonitized.

The metacherts consist predominantly of equigranular polygonal and irregular shaped quartz grains with small amounts of feldspar (plagioclase), micas, garnet, apatite, and opaque minerals. Although they have very weak foliation defined by the parallel arrangement of micas, they exhibit no clear lineation. Quartz and feldspar grains show no sign of shape preferred orientation. Thus, feldspar grains within the Yanazawa mylonite would allow assumption (2) to be made. As for garnet grains, a shape preferred orientation occurs weakly within metacherts in the Hongusan area, where the longest axis was vaguely oriented parallel to the plane of foliation. This will result in a more concentrated orientation pattern of garnet than that of feldspar when the metacherts deform plastically. The difference in the distribution patterns in the R/ϕ diagram between garnet and feldspar within the Yanazawa mylonite is presumably attributed to the difference in their initial orientation pattern. Hence, the distribution pattern of garnet grains within the Yanazawa mylonite (Fig. 16c) could violate assumption (2).

Assumption (3), that no porphyroclasts have changed their shape during deformation, may not be true, since the mylonitization of igneous rocks in the Kashio shear zone is known to be characterized by the grain size reduction of feldspar (Echigo & Kimura 1973, Takagi 1986). During mylonitization, the breaking and abrasion of feldspar grains would occur rather actively, and dynamic recrystallization at the margins of the porphyroclasts would also result in the grain size reduction of porphyroclasts. However, our analysis is not based on grain size but on grain shape. If effect of abrasion and dynamic recrystallization was equal all around the grains, this would not alter the aspect ratio, R. If the breaking of the many grains results statistically in similar preferred orientations of the long axes of the broken grains, it does not disturb the validity of the assumption (3). At the moment, we cannot prove nor disprove that assumption (3) is fulfilled in the mylonites.

Recently, a series of experiments in two dimensions demonstrated the influence of the concentration of particles on the development of a shape preferred orientation (Ildefonse & Fernandez 1988, Ildefonse *et al.* 1992a,b). Their result is that particle rotation is significantly disturbed when the distance between adjacent particles of equal size is shorter than their length. As the porphyroclasts within the two mylonites are adequately distant from neighbouring porphyroclasts, as shown in Figs. 14 and 15, assumption (4) is well satisfied for the mylonites.

As a consequence, our estimations of non-coaxiality for these mylonites are probably acceptable as a first approximation, and the deformation for the Yanazawa

mylonite proceeded under a relatively higher proportion of pure shear component (i.e. $\Theta = 40°$) than that for the Ohnishiyama mylonite (i.e. $\Theta = 20°$).

CONCLUDING REMARKS ON THE DEGREE OF NON-COAXIALITY

There are many methods available for estimating finite strain (e.g. Ramsay & Huber 1983). However, there has been less discussion of methods for estimating the degree of non-coaxiality (e.g. Passchier 1987, Vissers 1989, Cowan 1990, Wallis 1992). We emphasize that the analysis of shape preferred orientation of porphyroclasts demonstrated above is a possible method for determining the degree of non-coaxiality in shear zones.

The conclusion reached above indicates that deformation within the mylonites contains a certain amount of pure shear component superimposing on a simple shear component as $0° < \Theta < 40°$. Passchier (1987) estimated a kinematical vorticity number between 0.5 and 0.8, possibly 0.6 (corresponding to $15° < \Theta < 40°$) for his mylonite. Hanmer (1990) also pointed out that non-ideal shear deformation ($\Theta > 0°$) produced his mylonites. These examples strongly suggest that deformation of mylonites in many shear zones may be not ideal simple shear but general non-coaxial deformation with a pure shear component.

Acknowledgements—The authors wish to thank Ken-ichi Kano for critical comments, and Kazuo Kosaka for reading the earlier version of the manuscript. S. H. Treagus, J. van den Driessche and S. K. Ghosh are gratefully acknowledged for their constructive criticisms as well as improving the English. Part of this paper was financially supported by a Grant-in-Aid for Scientific Research from the Ministry of Education, Science and Culture, Japan to T. Masuda, and by an OPRS and a JCU Postgraduate Research Scholarship to K. Michibayashi.

REFERENCES

Berthe, D., Choukroune, P. & Jegouzo, P. 1979. Orthogneiss, mylonite and non-coaxial deformation of granites: the example of the South Armorican Shear Zone. *J. Struct. Geol.* **1**, 31–42.

Bouchez, J. L., Lister, G. S. & Nicolas, A. 1983. Fabric asymmetry and shear sense in movement zones. *Geol. Rdsch.* **72**, 401–419.

Cowan, D. S. 1990. Kinematic analysis of shear zones in sandstone and mudstone of the Shimanto belt, Shikoku, SW Japan. *J. Struct. Geol.* **12**, 431–441.

Dallmeyer, R. D. & Takasu, A. 1992. Middle Paleocene terrane juxtaposition along the Median Tectonic Line, southwest Japan: evidence from $^{40}Ar/^{39}Ar$ mineral ages. *Tectonophysics* **200**, 281–297.

Echigo, H. & Kimura, T. 1973. Minor geologic structures of the cataclastic rocks, including mylonites, along the Median Tectonic Line in the eastern Kii Peninsula, southwest Japan. In: *Median Tectonic Line* (edited by Sugiyama, R.). Tokai University Press (in Japanese with English abstract) 115–137.

Ferguson, C. C. 1979. Rotation of elongate rigid particles in slow non-Newtonian flows. *Tectonophysics* **60**, 247–262.

Gay, N. C. 1968. The motion of rigid particles embedded in a viscous fluid during pure shear deformation of the fluid. *Tectonophysics* **5**, 81–88.

Ghosh, S. K. 1987. Measure of non-coaxiality. *J. Struct. Geol.* **9**, 111–113.

Ghosh, S. K. & Sengupta, S. 1973. Compression and simple shear of test models with rigid and deformable inclusions. *Tectonophysics* **17**, 133–175.

Ghosh, S. K. & Ramberg, H. 1976. Reorientation of inclusions by combination of pure shear and simple shear. *Tectonophysics* **34**, 1–70.

Hanmer, S. 1990. Natural rotated inclusions in non-ideal shear. *Tectonophysics* **149**, 245–255.

Hanmer, S. & Passchier, C. 1991. Shear-sense indicators: a review. Geological Survey of Canada Paper 90–17.

Hayama, Y. & Yamada, T. 1980. Median Tectonic Line at the stage of its origin in relation to plutonism and mylonitization in the Ryoke belt. *Mem. geol. Soc. Japan* **18**, 5–26.

Hayashi, M. & Takagi, H. 1987. Shape fabric of recrystallized quartz in the mylonites along the Median Tectonic Line, southern Nagano Prefecture. *J. geol. Soc. Japan* **93**, 349–359 (in Japanese with English abstract).

Hooper, R. J. & Hatcher, R. D., Jr. 1988. Mylonites from the Towaliga fault zone, central Georgia: products of heterogeneous non-coaxial deformation. *Tectonophysics* **152**, 1–17.

Ildefonse, B., Launeau, P., Fernandez, A. & Bouchez, J. L. 1992a. Effect of mechanical interactions on development of shape preferred orientations: a two-dimensional experimental approach. *J. Struct. Geol.* **14**, 73–83.

Ildefonse, B. & Fernandez, A. 1988. Influence of the concentration of rigid markers in a viscous medium on the production of preferred orientations. An experimental contribution, 1. Non coaxial strain. In: *Geological Kinematics and Dynamics* (edited by Talbot, C. J.). *Bull geol. Inst. Univ. Uppsala* **14**, 55–60.

Ildefonse, B., Sokoutis, D. & Mancktelow, N. S. 1992b. Mechanical interactions between rigid particles in a deforming ductile matrix. Analogue experiments in simple shear flow. *J. Struct. Geol.* **14**, 1253–1266.

Jeffery, G. B. 1922. The motion of ellipsoidal particles immersed in a viscous fluid. *Proc. R. Soc. London, Ser. A* **102**, 161–179.

Leal, L. G. 1975. The slow motion of slender rod-like particles in a second-order fluid. *J. Fluid Mech.* **69**, 305–337.

Lister, G. S. & Snoke, A. W. 1984. *S–C* mylonites. *J. Struct. Geol.* **6**, 617–638.

Masuda, T., Koike, T., Yuko, T. & Morikawa, T. 1991. Discontinuous grain growth of quartz in metacherts: the influence of mica on a microstructural transition. *J. metamorphic Geol.* **9**, 389–402.

Means, W. D., Hobbs, B. E., Lister, G. S. & Williams, P. F. 1980. Vorticity and non-coaxiality in progressive deformation. *J. Struct. Geol.* **2**, 371–378.

Michibayashi, K. & Masuda, T. 1993. Shearing during progressive retrogression in the granitoids: abrupt grainsize reduction of quartz at the plastic–brittle transition for feldspar. *J. Struct. Geol.* **15**, 1421–1432.

Miyashiro, A. 1973. *Metamorphism and Metamorphic Belts*. George Allen and Unwin, London.

Mizutani, S. 1987. Mesozoic terranes in the Japanese Islands and neighbouring East Asia. *A.G.U. Geodynamic Series* **19**, 263–273.

Muskhelishvili, N. I. 1953. *Some Basic Problems of the Mathematical Theory of Elasticity*. Noordhoff, Groningen.

Nadai, A. 1963. *Theory of Flow and Fracture of Solids*. Engineering Societies Monographs. McGraw-Hill, New York.

Nicolas, A. & Poirier, J. P. 1976. *Crystalline Plasticity and Solid State Flow in Metamorphic Rocks*. Wiley, New York.

Oertel, G. 1985. Reorientation due to grain shape. In: *Preferred Orientation in Deformed Metals and Rocks: An Introduction to Modern Texture Analysis* (edited by Wenk, H.-R.). Academic Press, 259–265.

Passchier, C. W. 1986. Flow in natural shear zones—the consequences of spinning flow regimes. *Earth Planet. Sci. Lett.* **77**, 70–80.

Passchier, C. W. 1987. Stable positions of rigid objects in non-coaxial flow—a study in vorticity analysis. *J. Struct. Geol.* **9**, 679–690.

Passchier, C. W. 1991. The classification of dilatant flow types. *J. Struct. Geol.* **13**, 101–104.

Passchier, C. W. & Simpson, C. 1986. Porphyroclast systems as kinematic indicators. *J. Struct. Geol.* **8**, 831–843.

Ramsay, J. G. & Huber, M. I. 1983. *The Techniques of Modern Structural Geology, Vol. 1: Strain Analysis*. Academic Press, London.

Ramsay, J. G. & Huber, M. I. 1987. *The Techniques of Modern Structural Geology, Vol. 2: Folds and Fractures*. Academic Press, London.

Reed, J. L. & B. Tryggvason, E. 1974. Preferred orientation of rigid particles in a viscous matrix deformed by pure shear and simple shear. *Tectonophysics* **24**, 85–98.

Shibata, K. & Takagi, H. 1987. Isotopic ages of rocks and intrafault materials along the Median Tectonic Line: an example in the Bungui–Toge area, Nagano Prefecture. *J. geol. Soc. Japan* **94**, 35–50 (in Japanese with English abstract).

Simpson, C. & Schmid, S. 1983. An evaluation of criteria to deduce the sense of movement in sheared rocks. *Bull. geol. Soc. Am.* **94**, 1281–1288.

Takagi, H. 1986. Implications of mylonitic microstructures for the geotectonic evolution of the Median Tectonic Line, central Japan. *J. Struct. Geol.* **8**, 3–14.

Takagi, H. & Ito, M. 1988. The use of asymmetric pressure shadows in mylonites to determine the sense of shear. *J. Struct. Geol.* **10**, 347–360.

Vissers, R. L. M. 1989. Asymmetric quartz *c*-axis fabrics and flow vorticity: a study using rotated garnets. *J. Struct. Geol.* **11**, 231–244.

Wallis, S. R. 1992. Vorticity analysis in a metachert from the Sanbagawa Belt, SW Japan. *J. Struct. Geol.* **14**, 271–280.

Willis, D. G. 1977. A kinematic model of preferred orientation. *Bull. geol. Soc. Am.* **88**, 883–894.

Yamamoto, H. 1994. Kinematics of mylonitic rocks along the Median Tectonic Line, Akaishi Range, central Japan. *J. Struct. Geol.* **16**, 61–70.